frontiers | Frontiers in Remote Sensing

TYPE Original Research
PUBLISHED 15 January 2026
DOI 10.3389/frsen.2025.1732414

Check for updates

OPEN ACCESS

EDITED BY
Ahmet Cilek,
Çukurova University, Türkiye

REVIEWED BY
Digvesh Kumar Patel,
Indira Gandhi National Tribal University, India
Lakkur Gurunarayan Santhosh,
Ramaiah Institute of Technology, India

*CORRESPONDENCE
Sneha Gautam,
snehagautam@karunya.edu
Chang-Hoi Ho,
hoch@ewha.ac.kr

RECEIVED 25 October 2025
REVISED 04 December 2025
ACCEPTED 08 December 2025
PUBLISHED 15 January 2026

CITATION
Harani P, Gautam S, Joshi SK and Ho C-H (2026) Spatio-temporal analysis of land use transformations and their environmental implications in the Thamirabarani River Basin, India.
Front. Remote Sens. 6:1732414.
doi: 10.3389/frsen.2025.1732414

COPYRIGHT
© 2026 Harani, Gautam, Joshi and Ho. This is an open-access article distributed under the terms of the Creative Commons Attribution License (CC BY). The use, distribution or reproduction in other forums is permitted, provided the original author(s) and the copyright owner(s) are credited and that the original publication in this journal is cited, in accordance with accepted academic practice. No use, distribution or reproduction is permitted which does not comply with these terms.

Spatio-temporal analysis of land use transformations and their environmental implications in the Thamirabarani River Basin, India

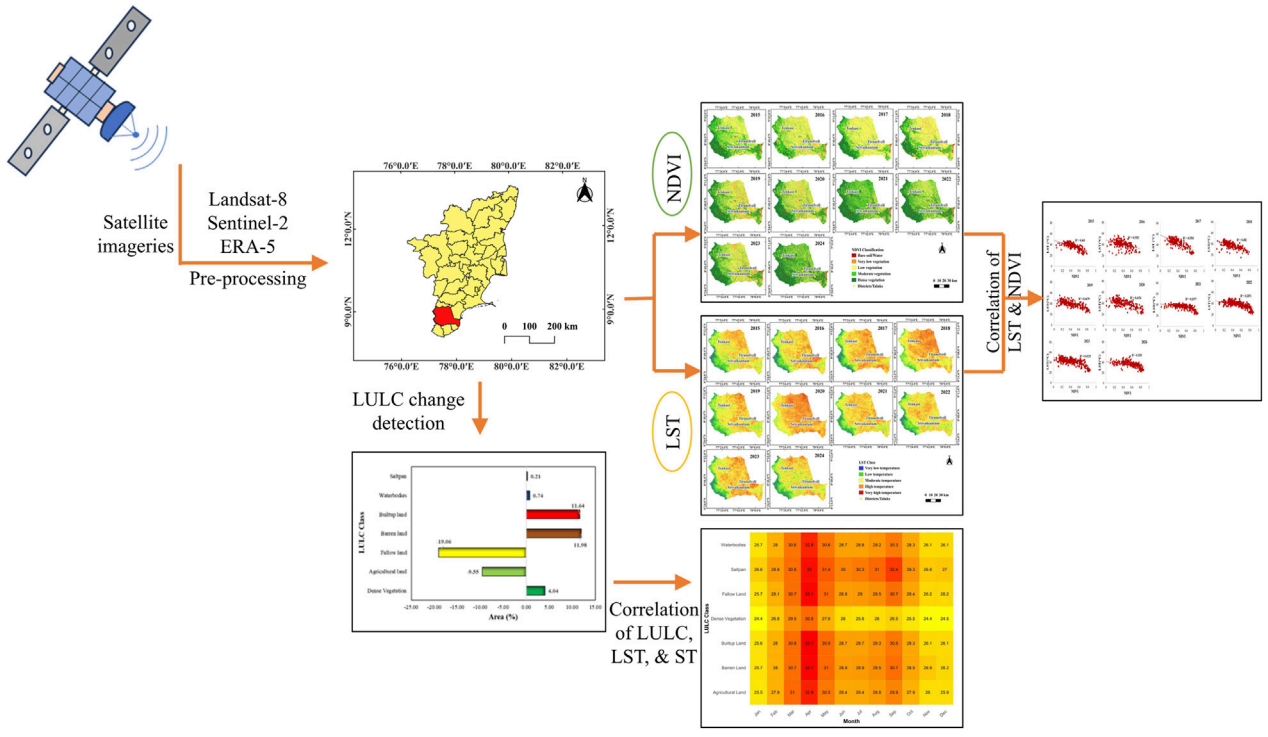
P. Harani[1], Sneha Gautam[1,2,3]*, Suneel Kumar Joshi[4] and Chang-Hoi Ho[3]*

[1]Division of Civil Engineering, Karunya Institute of Technology and Sciences Coimbatore, Coimbatore, Tamil Nadu, India, [2]Water Institute, A Centre of Excellence, Karunya Institute of Technology and Sciences, Coimbatore, Tamil Nadu, India, [3]Department of Climate and Energy Systems Engineering, Ewha Womans University, Seoul, Republic of Korea, [4]Geo Climate Risk Solutions Pvt. Ltd., Visakhapatnam, Andhra Pradesh, India

Rapid population growth and associated land-use/land-cover (LULC) transformations exacerbate environmental stress on natural resources, underscoring the importance of continuous monitoring to support sustainable land and water management. This study examines the spatio-temporal dynamics of LULC changes and the interrelationships among LULC, the normalized difference vegetation index (NDVI), land surface temperature (LST), and soil temperature (ST) in the Thamirabarani River Basin in Tamil Nadu, India. Multi-temporal satellite datasets from Landsat-8 (30 m resolution) and Sentinel-2 (10 m resolution) were processed in Google Earth Engine for the period from 2015 to 2024. The change detection analysis presented significant increases in built-up areas (11.6%) and barren land (11.9%), indicating rapid urbanization and progressive land degradation. NDVI analysis showed a significant positive long-term trend across the basin (slope = 0.00055, p = 0.0369), reflecting seasonal and interannual vegetation variability. Although, spatial analysis revealed a stable vegetation condition across the basin, minor reduction in vegetation was observed in urban and degraded areas, where the expansion of built-up and barren land has led to localized vegetation loss. Analyses of LST and ST showed substantial seasonal variations, indicating the critical role of vegetation cover in regulating land-atmosphere energy exchanges. NDVI exhibited a negative correlation with LST (R^2 = 0.15-0.55), reflecting the cooling effect of vegetation which reduces surface heating through canopy shading and enhanced evapotranspiration. This suggests that vegetation activity partially controls LST and ST. The present results demonstrate the urgent need to implement integrated, sustainable land and water management strategies, including promoting climate-resilient agricultural practices, regulating urban expansion, and implementing systematic vegetation restoration programs, to maintain ecosystem stability and resilience in the basin under intensifying climatic and anthropogenic pressures.

KEYWORDS

google earth engine, land surface temperature, land use/land cover change, satellite data, vegetation dynamics



GRAPHICAL ABSTRACT

1 Introduction

Accelerated demographic expansion and intensifying anthropogenic pressures have triggered unprecedented rates of land use/land cover (LULC) transformation and generated numerous impacts on ecosystem services, including biodiversity conservation, climate regulation, hydrological cycles, soil fertility, and food security (Ho et al., 2012; Jeong et al., 2014; Patil and Panhalkar, 2023; Yaghoobi et al., 2022). Human-environment interactions are particularly complex in developing regions, where rapid urbanization, agricultural expansion, and industrial development converge to exert multifaceted pressures on natural resource systems. LULC classification and change detection methodologies provide essential analytical frameworks for quantifying and characterising dynamic surface processes, including urban sprawl, deforestation, agricultural intensification, wetland degradation, and land abandonment, thereby enabling robust monitoring of landscape change across global scales (Loukika et al., 2021; Rehman et al., 2022; Thakur et al., 2025a). Such monitoring capabilities are critical for addressing interconnected global environmental concerns, including soil erosion, hydrological extremes (flooding and drought), biodiversity loss, carbon cycle disruption, and climate change adaptation, while also supporting evidence-based urban planning and sustainable land management strategies (Gaur and Singh, 2023; IPCC, 2023). Arid and semi-arid regions cover one-third of the global terrestrial surface, and are highly sensitive to land use and climate change (Bento et al., 2020).

Accurate LULC mapping and change detection are fundamental prerequisites for effective water resource planning, groundwater assessment, agricultural monitoring, and ecosystem service valuation (Khan A et al., 2025; Pande et al., 2024). Therefore, LULC change detection has become a key area of research in climate change science, natural resource management, and sustainable development planning over the past few decades (Asnawi et al., 2024; Binh et al., 2021). While traditional LULC mapping approaches based on analogue cartographic methods and extensive field surveys provide high reliability and ground-truth accuracy, they are inherently limited by substantial costs, labour requirements, temporal constraints, and restricted spatial coverage (Aldiansyah and Saputra, 2023). Revolutionary advances in remote sensing technologies, geographic information systems (GIS), and machine learning (ML) algorithms have addressed these methodological constraints, providing transformative alternatives. These alternatives enable rapid, cost-effective, and extensive classification of LULC with enhanced accuracy and reproducibility (Pande, 2022). Remote sensing platforms incorporating multispectral, hyperspectral, and synthetic aperture radar sensors provide multisource, multitemporal, and multiresolution datasets that are essential for monitoring LULC dynamics across different spatial and temporal scales (Jackson et al., 2025; Mansourmoghaddam et al., 2023).

The evolution of classification methodologies has progressed from conventional statistical approaches to sophisticated ML frameworks. While traditional unsupervised clustering algorithms (e.g., K-means and ISODATA) and parametric supervised classifiers (e.g., maximum likelihood and minimum distance) are

computationally efficient and interpretable, they perform poorly when processing high-dimensional spectral data, mixed pixels, and complex landscape heterogeneity (Jangid et al., 2023; Talukdar et al., 2020) In contrast, non-parametric supervised ML algorithms (including K-nearest neighbor, support vector machines, random forests, artificial neural networks, and regression trees) achieve higher accuracies by capturing complex data structures without assuming statistical data distribution (Abbas and Jaber, 2020; Tassi et al., 2021). Despite their strengths, these methods demand large volumes of training data and substantial computational resources, especially for generating land cover maps over extensive areas (Pan et al., 2022; Qu et al., 2021). The development of cloud-based geospatial platforms such as Google Earth Engine (GEE) has revolutionised Earth observation science by making petabyte-scale satellite archives and high-performance cloud computing infrastructure more accessible (Feizizadeh et al., 2023; Jamei et al., 2022; Khachoo et al., 2024). GEE's integrated processing environment facilitates the real-time analysis of multi-temporal, multi-spectral datasets while eliminating the need for labour-intensive preprocessing such as atmospheric correction, mosaicking, resampling, and coordinate system transformations (Shafizadeh-Moghadam et al., 2021; Pokhariya et al., 2023). The portability and operational efficiency of GEE provide an opportunity to analyze land cover changes, vegetation and temperature variations (Liu et al., 2025). Seamless integration with advanced remote sensing and geographic information system methodologies has enabled the efficient, scalable, and temporally consistent monitoring of global and regional LULC dynamics across multiple spatial scales (Nigar et al., 2024).

Beyond land cover mapping, LULC transitions influence land surface temperature (LST) and soil temperature (ST), critical biophysical parameters that regulate land-atmosphere energy exchanges and surface-subsurface thermal coupling (Guechi et al., 2021). LST is a key indicator used to assess surface energy balance dynamics, climate feedback mechanisms, and ecosystem-atmosphere interactions (El Garouani et al., 2021; Wang et al., 2024). Urban environments, characterised by impervious surfaces and reduced vegetation cover, exhibit high LST values (Park et al., 2017; Park et al., 2018). This intensifies urban heat island effects and alters local climate conditions (Hu et al., 2023; Nse et al., 2020; Patel et al., 2024a). ST represents the subsurface thermal regime and is affected by atmospheric conditions, soil moisture content, vegetation canopy structure, and land management practices.

Vegetated landscapes have lower ST values than bare or urbanized surfaces due to shading and evapotranspiration cooling processes (Jeong et al., 2009). Vegetation indices like the normalized difference vegetation index (NDVI) provide robust indicators for investigating vegetation-temperature relationships and ecosystem health status. NDVI quantifies vegetation cover density and photosynthetic activity, capturing seasonal phenological cycles, soil moisture dynamics, and agricultural productivity patterns (Sohail et al., 2023; Patel et al., 2024b). LST-NDVI relationship is influenced by various factors such as dense vegetation, dry soil, wetlands, rock surfaces, and waterbodies, which largely depend on seasonal variations (Guha and Govil, 2021; Guha and Govil, 2022). LULC, LST, ST, and NDVI yield comprehensive insights into biophysical feedback mechanisms and support evidence-based strategies for environmental monitoring, sustainable agricultural planning, and climate adaptation measures (Zhang et al., 2021). Although previous studies have examined rainfall variability and hydrological extremes in the Thamirabarani River Basin (Mohan Kumar et al., 2022; Kaliraj et al., 2025), comprehensive spatiotemporal assessments integrating LULC dynamics, vegetation health, and thermal regimes remain lacking.

To address this gap, the present study investigates the Thamirabarani River Basin in Tamil Nadu, the only perennial river basin in the state, originating from the Pothigai Hills of the Western Ghats and discharging into the Gulf of Mannar near Punnaikayal in Thoothukudi district. It is the primary source of water supply for agricultural and domestic consumption in Southern Tamilnadu (Mohan Kumar et al., 2022). Anthropogenic climate change alters land-atmosphere-energy dynamics, leading to declining agricultural productivity and rising temperatures. Therefore, an integrated analysis of LULC, LST, NDVI, and ST is essential for developing adequate water and land management strategies. The research objectives are to: (1) quantify spatio-temporal LULC transformations for the period 2015, 2017, 2019, 2021, and 2024 using multi-sensor satellite data, (2) examine the statistical relationships between NDVI and thermal parameters (LST and ST), and (3) evaluate spatial patterns of LST and ST across different LULC categories to elucidate biophysical interactions with vegetation dynamics and land surface energy balance.

2 Materials and methods

2.1 Study area

The Thamirabarani River Basin is located in the south of Tamil Nadu, India, between 8°26′45″ N – 9°12′00″ N and 77°09′00″ E – 78°08′30″ E. It extends approximately 128 km in length with a variable width ranging from 20 to 85 km, and comprises a total watershed area of about 5,717 km^2. The basin spans significant portions of the Tirunelveli, Thoothukudi, and Tenkasi districts, thereby integrating diverse physiographic and land-use characteristics central to hydrological and soil resource studies. Figure 1 represents the study area map.

Hydrologically, the basin is regulated by a system of eight anicuts and eleven irrigation channels, which together constitute the backbone of agricultural water distribution over the region. The basin is further subdivided into seven principal sub-basins - Chittar, Uppodai, Gadana Nadhi, Manimuthar, Pachaiyar, Upper Thamirabarani, and Lower Thamirabarani. The western sector, encompassing the high-altitude Western Ghats, is dominated by dense forest cover that plays a vital role in sustaining the basin's hydrological regime. In contrast, the eastern region transitions progressively into fertile agricultural landscapes and low-lying coastal plains adjacent to the Gulf of Mannar. This spatial variation demonstrates a pronounced west-to-east gradient in physiography, land-use patterns, and water-resource dependency.

Climatically, the basin receives 986 mm of annual rainfall, influenced by the Southwest monsoon (June to September) and the Northeast monsoon (October to December). The temperature varies with the seasons, with an average maximum temperature of 31.6 °C during the peak summer months (April to August), accompanied by a mean relative humidity of 71.7% and an

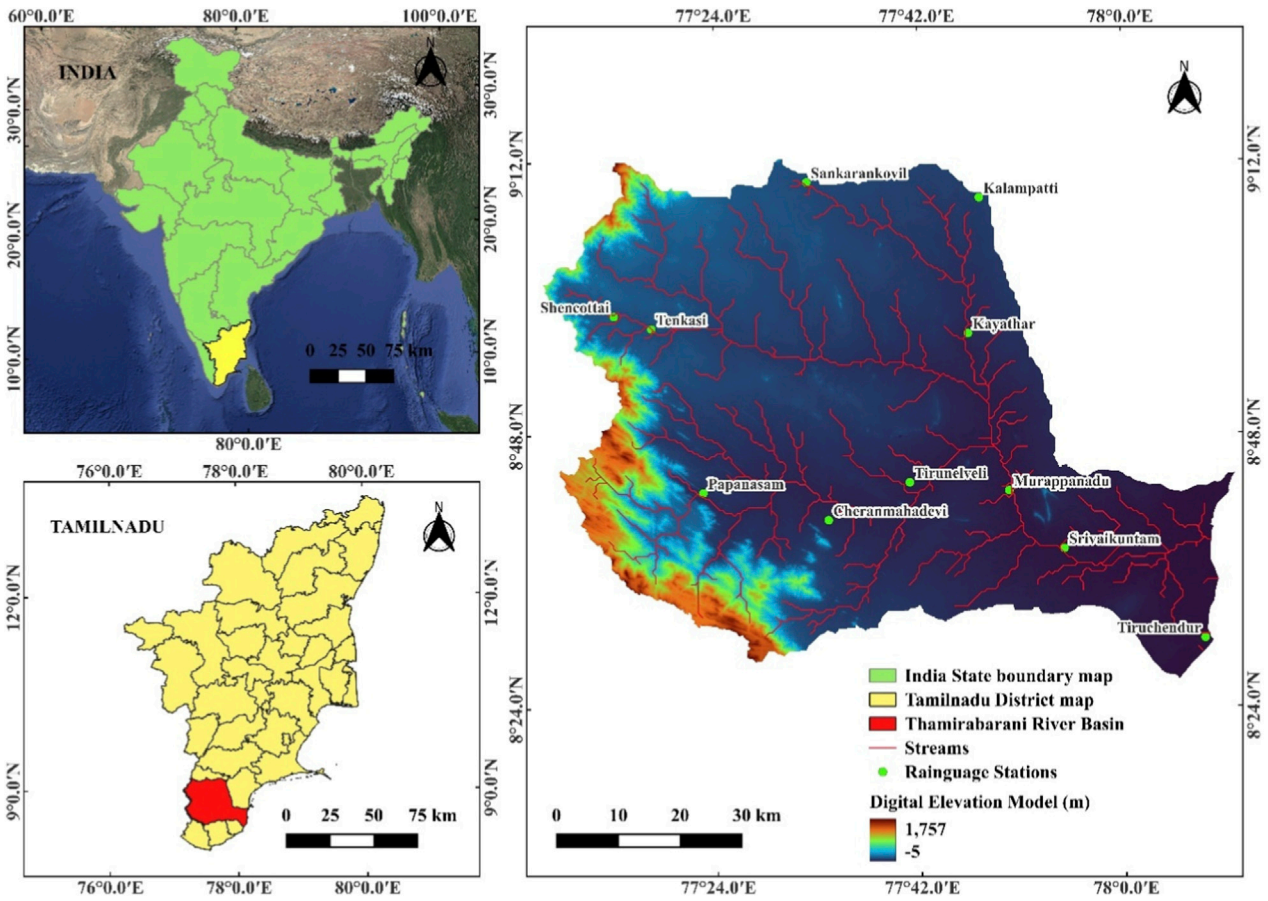


FIGURE 1
Location map of the Thamirabarani River Basin in Tamil Nadu, India. The basin boundary and drainage network are delineated using the Shuttle Radar Topography Mission Digital Elevation Model (SRTM-DEM, 30 m resolution), with surface elevations ranging from −5 m to 1,757 m. The spatial distribution of rain gauge stations indicates the observational network. The map is referenced to the WGS 84 coordinate system and includes a north arrow and a scale bar to facilitate spatial orientation.

average of 6.3 h of sunshine per day. According to the National Water Commission (2017), these hydro-meteorological conditions significantly influence water availability, agricultural productivity, and ecological dynamics in the basin. This highlights the vital role of seasonal monsoon variability in regulating the sustainability of regional resources.

2.2 Datasets

A vast repository of Earth Observation datasets is accessible via the GEE platform (https://code.earthengine.google.com/), which combines multi-sensor and multi-temporal satellite archives to support large-scale environmental monitoring and analysis. In this study, LULC, NDVI, and LST products are retrieved from GEE. Landsat-8 Operational Land Imager (OLI) and Sentinel-2 Multi-Spectral Instrument (MSI) datasets, provided by the United States Geological Survey (USGS) and the European Space Agency (ESA)/Copernicus Programme, respectively, are used for LULC and NDVI analyses. ST data were obtained from the ERA5-Land reanalysis product, curated by the European Centre for Medium-Range Weather Forecasts (ECMWF) and distributed via the Copernicus Climate Data Store.

Geospatial analyses and cartographic mapping were conducted in QGIS (Quantum GIS, an open-source GIS software) and ArcGIS (a GIS software developed by Environmental Systems Research Institute) to complement outputs derived from GEE. Standard pre-processing routines were applied in GEE to ensure data integrity and spatial harmonisation, including cloud masking, mosaicking, median band compositing, and clipping to the study extent (Feng et al., 2022; Gündüz, 2025). Table 1 summarises the satellite datasets employed for LULC, NDVI, LST and ST assessments.

2.2.1 NDVI estimation

Landsat-8 and sentinel-2 images were collected from GEE with a cloud cover of ≤10% for NDVI estimation. The NDVI is one of the most widely used metrics for assessing vegetation condition and dynamics (Gunawan et al., 2023; Thakur et al., 2025b). It exploits the strong contrast between the near-infrared (NIR) and red reflectance bands to quantify vegetation greenness, with values theoretically ranging from −1 to +1 (Gelata et al., 2023). Healthy vegetation reflects more NIR and green light while absorbing more blue and red

TABLE 1 Description of Satellite data collection.

Parameters	Datasources	Resolution
LULC	USGS Landsat-8/Collection-2/Tier-1/Level-2 [2015, 2017]	30 m
	ESA/Copernicus harmonized Sentinel-2 MSI: Multispectral instrument, Level-2A (SR) [2019, 2021, 2024]	10 m
NDVI	USGS Landsat-8/Collection-2/Tier-1/toa reflectance [2015–2018]	30 m
	ESA/Copernicus harmonized Sentinel-2 MSI: Multispectral instrument, Level-2A (SR) [2019–2024]	10 m
LST	USGS Landsat-8/Collection-2/Tier-1/Level-2 [2015–2024]	30 m
ST	ERA5-Land/Copernicus climate data store [2015–2024]	~9 km
SRTM-DEM	USGS Earth Explorer	30 m

light (Sharmin et al., 2024). High NDVI values are associated with healthy, dense vegetation, whereas low or negative values correspond to non-vegetated surfaces such as water bodies, bare soil, snow, or cloud cover (Guha et al., 2020a; Sharma et al., 2022).

2.2.2 LST estimation

The collection of Landsat eight surface reflectance images was conducted from GEE with a cloud cover of ≤10%. Surface temperature band (ST_10), i.e., Band 10 from the Landsat 8/9 Thermal Infrared Sensor, were used for retrieving LST. The ST_10 band is scaled using scaling factors and converted from Kelvin to Celsius. Vegetation conditions were characterized using the NDVI, computed from surface reflectance band SR_B4 (red band) and SR_B5 (NIR band). The proportion of vegetation cover (Pv) was calculated using Equation 1, with threshold values of $NDVI_{min}$ = 0.2 and $NDVI_{max}$ = 0.5 (Ermida et al., 2020).

$$Pv = \frac{(NDVI - NDVI_{min})}{(NDVI_{max} - NDVI_{min})} \quad (1)$$

where $NDVI_{min}$ is minimum NDVI value within the study area, and $NDVI_{max}$ is maximum NDVI value within the study area. Surface emissivity (Ɛ) values were calculated using Equation 2:

$$Ɛ = 0.004Pv + 0.986 \quad (2)$$

LST (°C) was derived using a mono-window algorithm (Imroah and Setiawan, 2024; Njoku and Tenenbaum, 2022) from Equation 3:

$$LST = \frac{T_b}{1 + \left(\lambda.\frac{T_b}{\rho}\right)\ln(Ɛ)} - 273.15 \quad (3)$$

where λ is wavelength of emitted radiance, T_b is brightness temperature, Ɛ is emissivity, and ρ is constant (1.4388 m K).

2.2.3 Soil temperature estimation

Monthly ST gridded data with a native spatial resolution of ~9 km and latitude-longitude grid resolution of 0.1 ° × 0.1 ° were obtained from the ERA5-land reanalysis product at a soil depth of 0–7 cm, which is available via the Copernicus Climate Data Store for the period 2015–2024. The datasets were converted to a compatible format and clipped to the study area in ArcGIS. Missing values were corrected using Inverse Distance Weighting (IDW) interpolation, after which ST maps were generated for each month. The extracted raster was then used for a correlation analysis across different LULC classes.

2.3 Methodology

This section describes the methods involved in the pre-processing of satellite imagery, estimation of NDVI, LST, ST, and LULC classification. The detailed methodology is depicted in Figure 2. In particular, the LULC classification process is described below. An annual image collection of (Landsat-8 and Sentinel-2) was compiled using median composites for 2015, 2017, 2019, 2021, and 2024. These annual composites were used further for spatial analysis of LULC, NDVI, and LST, representing year-wise conditions.

Furthermore, all monthly images from 2015 to 2024 were used to assess the correlation between LULC and LST. Similarly, ERA5-land monthly ST data were obtained for 2015 and 2024 to determine the relationship between ST and each LULC class. Correlation analysis of LULC and LST, LULC and ST were computed using Python programming, and spatial maps were generated using QGIS software.

Among medium-resolution images, Landsat-8 and Sentinel-2 provided high temporal resolution, short revisit periods, and broad spectral coverage (Nasiri et al., 2022; Nikkala et al., 2022). LULC change dynamics were analysed for 2015, 2017, 2019, 2021, and 2024 to examine the major land-use transitions in the Thamirabarani River Basin. All imagery was spatially subset to the basin extent and temporally filtered to maintain a maximum cloud cover remained below 10%. Median composites of the selected scenes were then generated to reduce atmospheric noise, seasonal variability, and residual cloud contamination.

Classification was supported using spectral bands (Band 2 – Band 7) from Landsat-8 and (Band 2–Band 8, Band 11, and Band 12) from Sentinel-2, which provide comprehensive coverage across the visible, NIR, and shortwave infrared (SWIR) domains of the electromagnetic spectrum (Ngondo et al., 2021). To further improve classification accuracy, a set of spectral indices was integrated as ancillary variables: NDVI for monitoring vegetation, Normalized Difference Built-up Index (NDBI) for detecting built-up and impervious surfaces, Modified Normalized Difference Water Index (MNDWI) for effectively extracting water bodies, and Enhanced Vegetation Index (EVI) for enhancing vegetation discrimination by minimising the effects of the atmosphere and soil background (Abdalkadhum et al., 2021; Gunduz, 2025; Patel S. et al., 2024). The combined use of spectral bands and indices substantially improved the separability of land cover classes, thereby strengthening the robustness and reliability of the

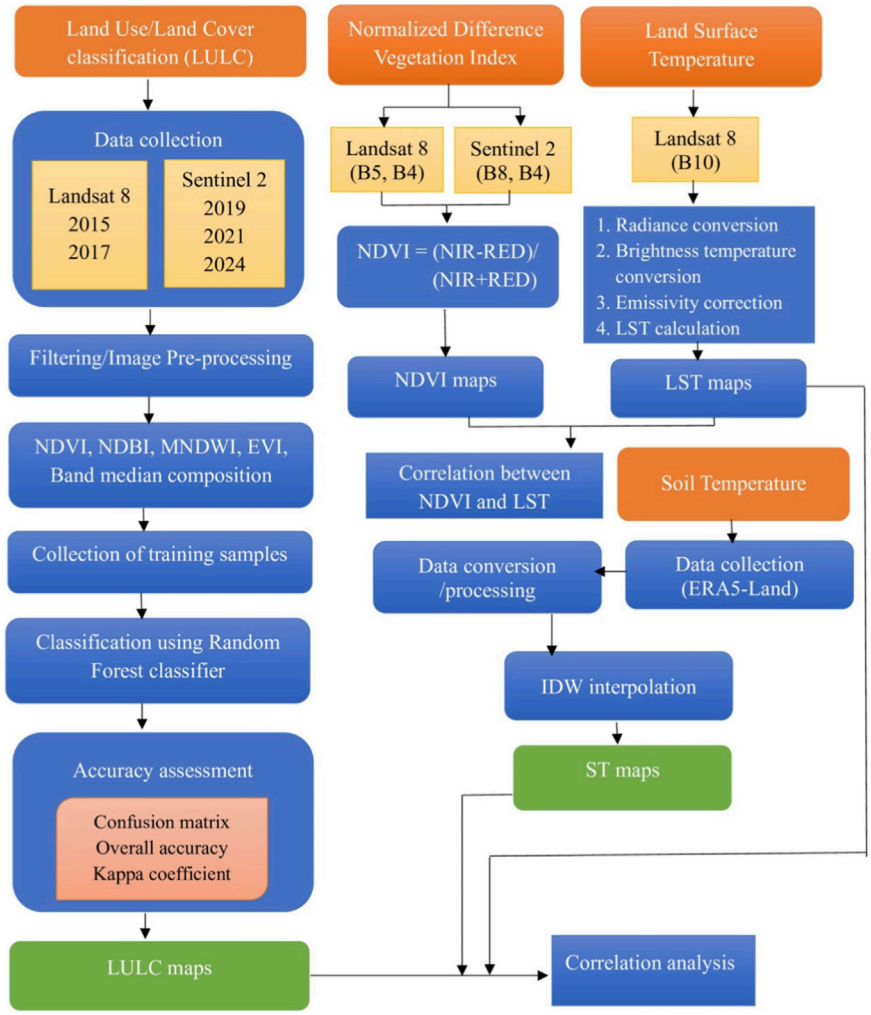


FIGURE 2
Methodological framework for land use, vegetation, and temperature mapping. The study uses various satellite datasets (Landsat-8 and Sentinel-2) to monitor the change in LULC, vegetation, LST, and ST. Random Forest method was used to classify LULC and near infrared, red, and thermal bands are used to estimate NDVI and LST; whereas ST maps were generated from ERA-5 land gridded datasets. Correlation analysis was performed to examine the relationship among LULC, LST, ST, and vegetation index. For correlation analysis across different LULC classes, the datasets were spatially aggregated to match ~9 km resolution.

TABLE 2 Band information of satellite data used for LULC classification.

Datasets	Bands used
Landsat-8	Band 2 (blue), band 3 (green), band 4 (red), band 5 (NIR) Band 6 (SWIR 1), band 7 (SWIR 2)
Sentinel-2	Band 2 (blue), band 3 (green), band 4 (red), band 5 (red-edge 1), band 6 (red-edge 2), band 7 (red-edge 3), band 8 (NIR), band 11 (SWIR 1) Band 12 (SWIR 2)

classification results. A summary of the spectral bands employed to calculate NDVI, NDBI, MNDWI in this study were presented in Table 2.

As noted in previous studies, supervised classification requires robust, representative training and validation samples (Liu et al., 2020). For each reference period, training samples were randomly selected and subsequently merged into a unified dataset. A minimum of 50 samples was collected for each LULC category, after which a random column was generated to partition the dataset into training (80%) and validation (20%) subsets. The resulting training set was used to calibrate a Random Forest (RF) classifier. The LULC classification scheme was adapted from the National Remote Sensing Center (NRSC) standards and the National Water Mission report on the Thamirabarani River Basin (2017) to provide methodological consistency and regional relevance.

RF is an ensemble learning method that combines predictions from multiple decision trees and reduces computational time (Aldiansyah and Saputra, 2023). This algorithm produces accurate predictions by aggregating the outputs of individual trees (Nigar et al., 2024). The trained classifier was applied to composite imagery to generate LULC maps. For LULC classification, accuracy assessment is essential for evaluating model performance (Amini et al., 2022; Bar et al., 2020). An independent validation dataset comprising 20% of the total

samples was used for this purpose. The Kappa index is a widely used metric for assessing classification accuracy, while overall accuracy is used to validate image classification results (Digra et al., 2022; Tewabe and Fentahun, 2020). Overall accuracy (OA) and the Kappa coefficient (K) were calculated using a confusion matrix (Nasiri et al., 2022) via the following Equation 4 and Equation 5:

$$Overall\ Accuracy = \frac{Number\ of\ Correctly\ Classified\ Samples}{Number\ of\ Total\ Samples} \quad (4)$$

$$Kappa = \frac{Overall\ Accuracy - Estimated\ Chance\ Agreement}{1 - Estimated\ Chance\ Agreement} \quad (5)$$

Post-classification change detection is a widely used method for assessing temporal variations in LULC by comparing classified maps from different time periods. All LULC maps were harmonized to a common spatial resolution of 30 m before post-classification change detection. The Sentinel-2 derived LULC maps for 2019, 2021 and 2024 were resampled to 30 m using nearest neighbor resampling to match the resolution of Landsat-8 LULC maps (2015 and 2017), ensuring spatial consistency and improving the accuracy of change detection. In this study, QGIS plugin Modules for Land Use Change Evaluation (MOLUSCE) was used to analyse LULC transitions.

3 Results

3.1 Land use/land cover pattern

The spatial analysis of LULC change patterns was conducted for the Thamirabarani River Basin across 5-year periods: 2015, 2017, 2019, 2021, and 2024 as shown in Figure 3. The major LULC categories identified include agricultural land, fallow land, barren land, built-up land, dense vegetation, and water bodies. Notable fluctuations were observed across these land cover classes during the analysis period. The western and southwestern regions of the basin, which coincide with the Western Ghats, were characterised by dense vegetation and extensive forest cover. However, a sharp decline was recorded in 2017, when the forest area decreased from 826.20 km^2 to 518.04 km^2 as indicated in Figure 4a. This contraction corresponded to the deficient rainfall of 2016, a drought year that severely restricted vegetation growth. By 2019, dense vegetation cover had partially recovered due to agricultural expansion into forest margins, particularly for plantation crops such as sugarcane and paddy, supported by irrigation systems. However, this recovery was short-lived; by 2024, forest cover had again decreased from 1,291.91 km^2 to 1,057.49 km^2 as shown in Figure 4a, driven by conversion to settlements, agricultural fields, and barren land. Similar dynamic trends were evident in agricultural land, with declines observed in 2017 and 2019, likely linked to rainfall shortages. Subsequent expansions in 2021 and 2024 (from 1,510.02 km^2 to 1,590.41 km^2) demonstrated the resilience of agriculture as the primary source of livelihood in the basin. This pattern was evident in the Tirunelveli and Thoothukudi districts, where agriculture was sustained by two principal cropping seasons: Pishanam and Kar cultivation, supported by widespread irrigation systems for crops such as paddy, sugarcane, and banana.

From Figure 4a, it was evident that fallow land expanded considerably during the drought years, increasing from 1,445.44 km^2 in 2015 to 2,454.40 km^2 in 2017, as a result of large areas of agricultural land being temporarily left uncultivated due to prolonged dry conditions or soil fertility restoration practices. Meanwhile, barren land and the built-up regions show consistent increase throughout the study period, indicating ongoing urban expansion, infrastructure development, and land degradation. The extent of water bodies also showed strong dependency on climate. Reduced water availability in 2017 and 2019 coincided with mild to moderate drought conditions, resulting in decreased river discharge and storage capacity. In addition, the basin contains extensive saltpan areas, particularly in the downstream Thoothukudi district, which represents one of India's largest salt-producing regions. The extent of the saltpans varies seasonally due to controlled evaporation of seawater in shallow ponds. The temporal analysis showed that the Thamirabarani River Basin undergone dynamic LULC transitions over the past decade. These changes were primarily driven by climatic variability, including rainfall fluctuations and drought episodes, as well as anthropogenic activities such as agricultural intensification, urbanization, and industrial expansion. This emphasises the complex interplay between natural and human-induced processes in shaping the basin's landscape.

Consistent with these trend, agricultural and fallow land decreased significantly by 9.55% and 19.06%, respectively as shown in Figure 4b, indicating reductions in cultivable areas. These declines were linked to irregular rainfall patterns, land degradation processes, and urban development into agricultural zones. The trend in barren land was more complex, with a temporary contraction observed in 2021 (1,106.33 km^2) as indicated in Figure 4a. However, by 2024, barren land had expanded by 11.98% Figure 4b, indicative of intensified land degradation and vegetation loss. In contrast, built-up areas demonstrated steady and persistent expansion throughout the analysis period, with overall growth of 11.64% as shown in Figure 4b, underscoring the significant urbanization trajectory within the basin. Dense vegetation showed a modest increase of 4.04% from Figure 4b, which may be attributed to changes in canopy cover and climatic variation. The spatial extent of water bodies and saltpans shows modest increase during the analysis period primarily due to seasonal rainfall fluctuations, the construction of artificial storage structures, and coastal saltpan operations, particularly in downstream regions.

The reliability of the classification results can be confirmed through multi-temporal accuracy assessments. The overall accuracies achieved were 84.96% (2015), 80.91% (2017), 96.84% (2019), 97.86% (2021), and 91.97% (2024), with corresponding kappa coefficients of 0.81, 0.76, 0.89, 0.93, and 0.84, respectively. These values indicate a level of agreement ranging from strong to almost perfect between the classified outputs and the reference datasets. The results collectively validate the robustness and consistency of the classification framework: overall accuracies ≥80% verify the model's high reliability, and kappa statistics reinforce the scientific credibility of the LULC assessments across all temporal periods.

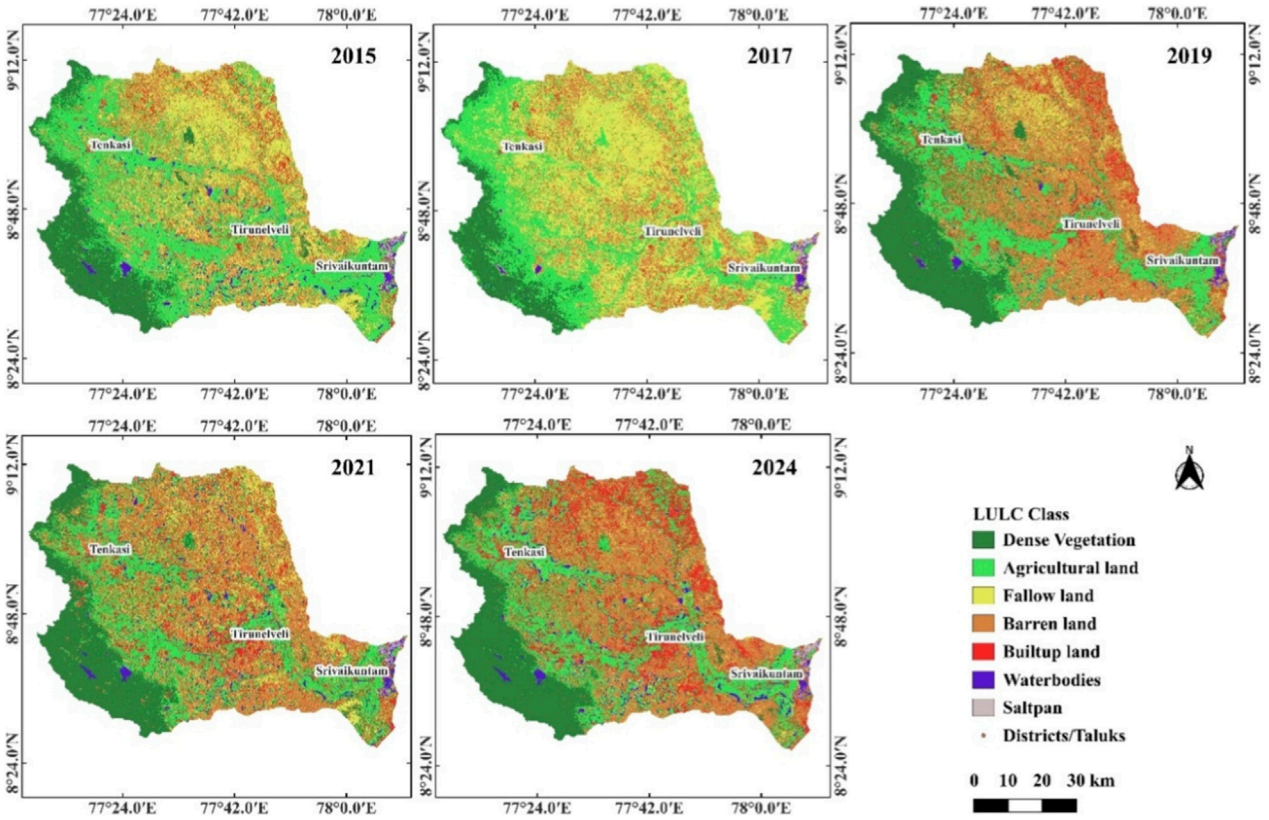


FIGURE 3
LULC pattern of Thamirabarani in 5 years (2015, 2017, 2019, 2021, and 2024)

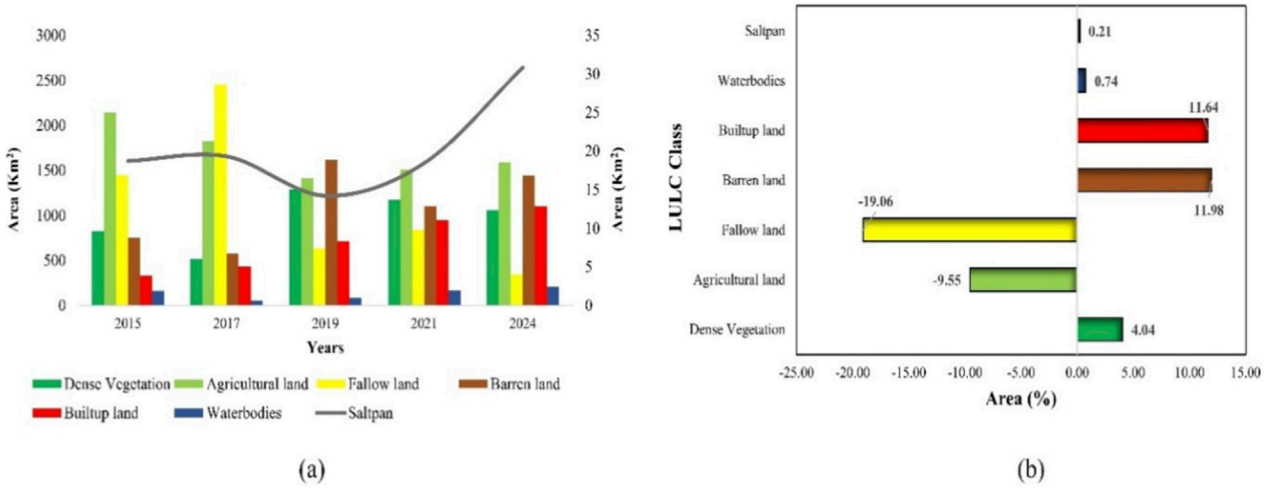


FIGURE 4
(a) Change in area for different LULC classes from 2015 to 2024. Both Y-axis represents the areal extent (km^2) of various LULC classes while, area of saltpan class is plotted on a secondary axis. As the area covered by saltpan is comparatively small, the values are scaled down (~100) for better visualization **(b)** Percentage change in LULC class between 2015 and 2024. Long term change detection represents the net change between initial and final years, which can be obtained through MOLUSCE plugin in QGIS.

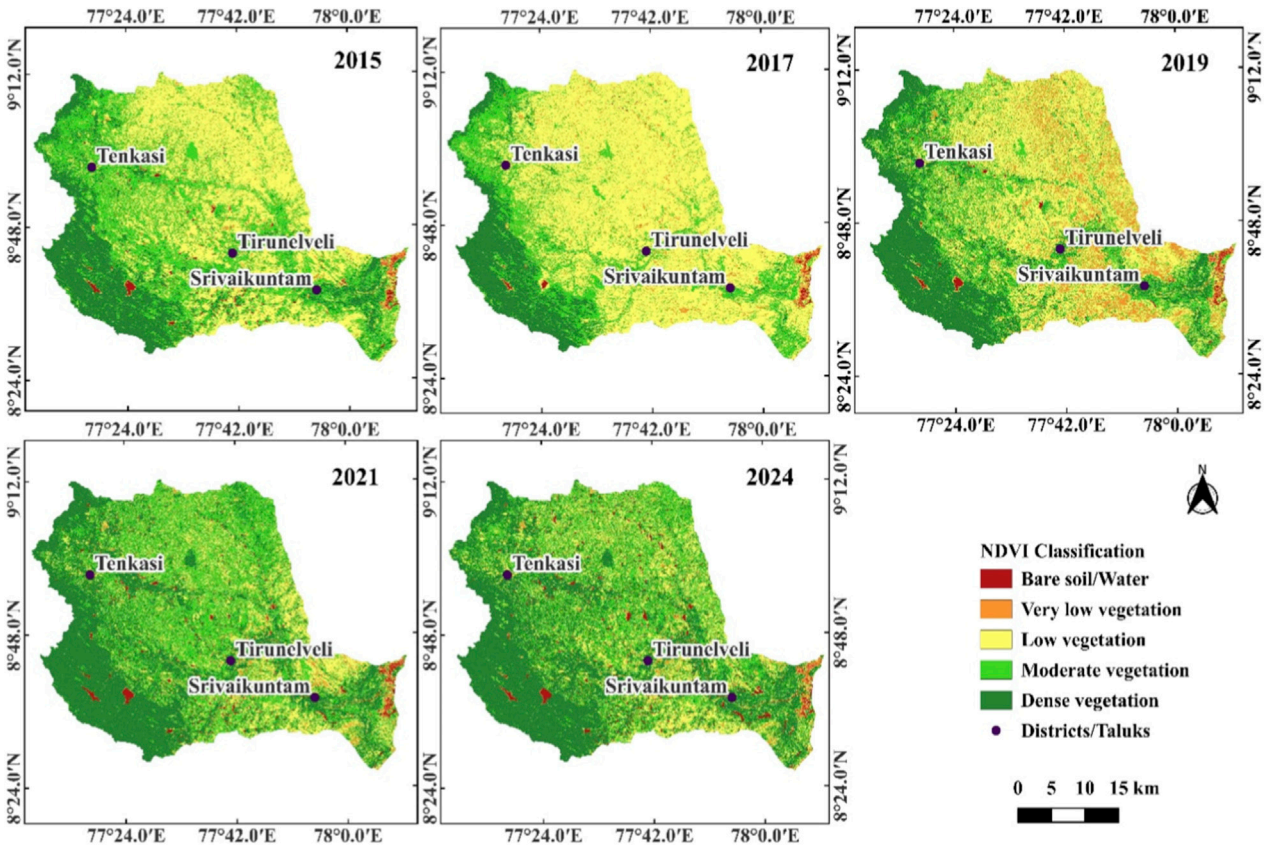


FIGURE 5
Annual average NDVI maps of Thamirabarani river basin in 5 years (2015, 2017, 2019, 2021, and 2024).

3.2 Spatial changes in NDVI

Figure 5 shows the annual average distributions of vegetation health in the Thamirabarani River Basin from 2015 to 2024. The NDVI analysis effectively captures seasonal vegetation dynamics, highlighting the close relationship between rainfall variability, cropping patterns, and vegetative cover. The upstream region, influenced by the Western Ghats, consistently supported dense vegetation, whereas the downstream coastal regions showed lower NDVI values due to the predominance of agricultural land, fallow land and scattered settlement areas. This spatial distribution corresponds with the northeast monsoon, which brings peak rainfall, and initiates the primary cropping season. In 2015 and 2017, the central part of the basin showed lower NDVI values, possibly due to moisture stress and post harvesting practices. In 2019, extensive areas within the basin recorded low to very low vegetation, likely linked to monsoon dryness, rainfall variability, cropping cycles, reduced soil moisture availability, and settlement expansion. By contrast, significant improvements in vegetation cover, ranging from moderate to dense, were observed in 2021 and 2024. This improvement coincided with favorable northeast monsoon rainfall, which replenished soil moisture and supported intensive agricultural activity. Overall, regions with persistently low NDVI values were associated with barren surfaces, sparse vegetation cover, and agricultural stress.

3.3 NDVI trend analysis

The mean NDVI was calculated from 2015 to 2024 and the corresponding long-term trend is shown in Figure 6. Sen's slope estimator, a non-parametric approach, was used to compute the slope of the trend line to evaluate the direction and extent of the change.

The temporal profile of NDVI showed a clear seasonal fluctuation, with peaks corresponding to periods of intense vegetative activity (e.g., cropping seasons) and troughs corresponding to phases of reduced vegetation cover. A sharp decline in NDVI values were observed in 2016 and 2017, coinciding with widespread vegetation stress caused by deficit monsoonal rainfall. Notably, 2016 was recognized as a drought year in the Thamirabarani River Basin, which substantially reduces vegetation growth. Between 2020 and 2024, NDVI exhibited greater variability, reflecting the combined influence of climatic fluctuations (e.g., rainfall and temperature anomalies) and land use changes. Despite this variability, the overall trajectory, represented by a sen's slope value of 0.00069, suggests a slight increase over the period. This positive shift may be linked to seasonal cropping cycles and intensified agricultural practices. However, vegetation remains ecologically stressed in urban and degraded areas, highlighting the dual pressures of climatic variability and anthropogenic disturbances. Statistical validation confirmed the reliability of the trend, with a p-value of 0.00829 (<0.01) and a 95% confidence

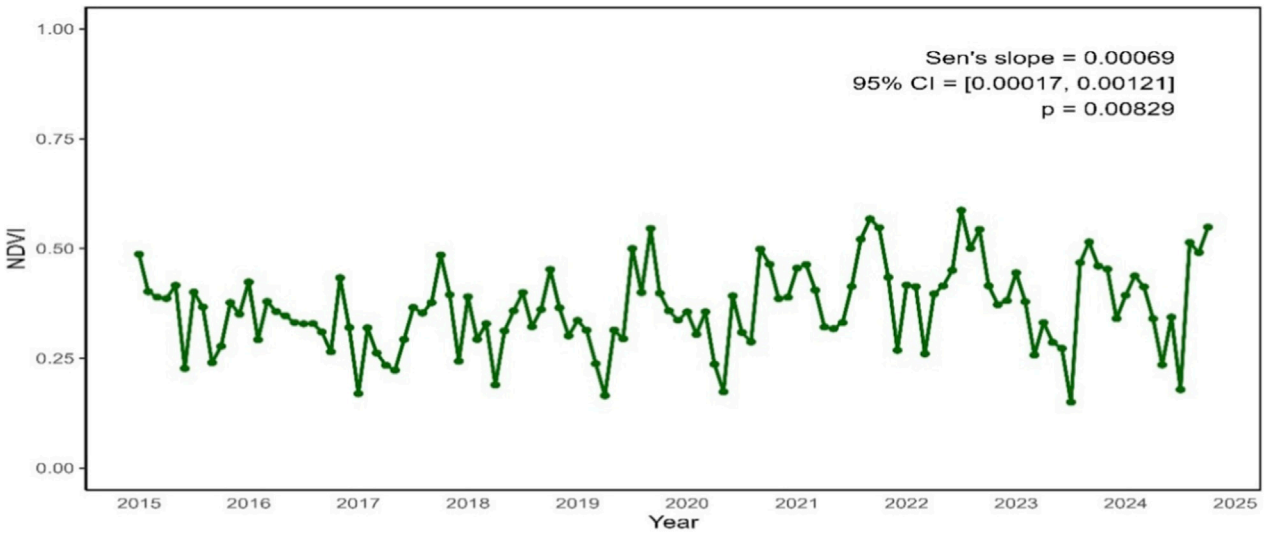


FIGURE 6
Trend analysis of NDVI in the Thamirabarani River Basin using monthly NDVI values.

interval (CI) of 0.00017–0.00121. This confirmed that the observed increase in NDVI was statistically significant.

3.4 Analysis of LST

Figure 7 illustrates the spatio-temporal variation of LST in the Thamirabarani River Basin during the years 2015, 2017, 2019, 2021, and 2024. The spatial distribution of LST across the basin shows that variability primarily influence by vegetation density, land cover characteristics, and topography. Coastal and vegetated regions were predominantly represented by green to blue shades, corresponding to lower surface temperatures. In contrast, barren surfaces, fallow lands and urbanized areas appeared in red to orange shades, indicating higher surface temperatures. The western portion of the basin, encompassing the forested hill regions of the Western Ghats, consistently experiences low to moderate temperatures, attributed to dense vegetation cover and cooler seasonal conditions.

In contrast, the basin's central part recorded moderate to high temperatures, representing zones of maximum heat stress due to reduced vegetation and exposure of barren and agricultural lands. In 2015 and 2017, the basin exhibited moderate to high LST values, consistent with reduced vegetation cover and limited soil moisture availability. In 2019, 2021, and 2024, low to moderate LST values were observed across much of the basin, with higher temperatures concentrated in saltpan areas, urban areas and localized barren patches, underscoring the thermal impact of anthropogenic activities and land degradation. By contrast, downstream coastal regions recorded relatively lower temperatures, likely moderated by marine influence. Overall, the results demonstrate that the combined effects of seasonal dynamics, land cover distribution, and topographic variation governed LST variability. The findings also emphasized the progressive warming of bare and urbanized areas, and shifts in land-use patterns.

3.5 Correlation analysis

3.5.1 Correlation between NDVI and LST

Figure 8 illustrates the relationship between NDVI and LST across different months. Pearson's correlation coefficient was used to analyze the correlation between LST and NDVI. NDVI and LST are very sensitive to climatic variations and changes in NDVI may alter the temperatures. Figure 8 confirms that NDVI has a negative correlation with LST during the year 2015 (R^2 = 0.46), 2017 (R^2 = 0.55), 2019 (R^2 = 0.46), 2021 (R^2 = 0.24), and 2024 (R^2 = 0.15), indicating that dense vegetation cover reduces surface temperature, likely due to relatively stable vegetation conditions. Areas with low vegetation exhibited higher surface temperatures, while densely vegetated areas exhibited lower surface temperatures, as vegetation reduces the amount of incoming radiation absorbed by the land surface and enhances evapotranspiration. However, moderate correlation during 2015 (R^2 = 0.46), 2017 (R^2 = 0.55), and 2019 (R^2 = 0.46), indicates that besides NDVI, other factors like topography, elevation, and local microclimatic conditions. In contrast, correlations for 2021(R^2 = 0.24) and 2022 (R^2 = 0.15) are weak, indicating that seasonal fluctuations, rainfall variability, and land surface heterogeneity weakened the vegetation-temperature relationship. Previous studies have reported that an R^2 value of ≥0.40 is generally required to establish a strong association between vegetation indices and thermal characteristics (Sohail et al., 2023; Rahimi et al., 2025). These results indicate that variations in NDVI correspond to changes in LST, reflecting vegetation's influence in regulating surface energy balance and land-atmosphere interactions. Numerous studies across various regions have reported such an inverse relationship between LST and NDVI (Thi Hong Ngoc et al., 2025; Anitha et al., 2023; Yue et al., 2007; Sajan et al., 2023).

3.5.2 Correlation between LULC and LST

Figure 9 presents the correlation between LST and different LULC classes across multiple months in 2015 and 2024. Due to

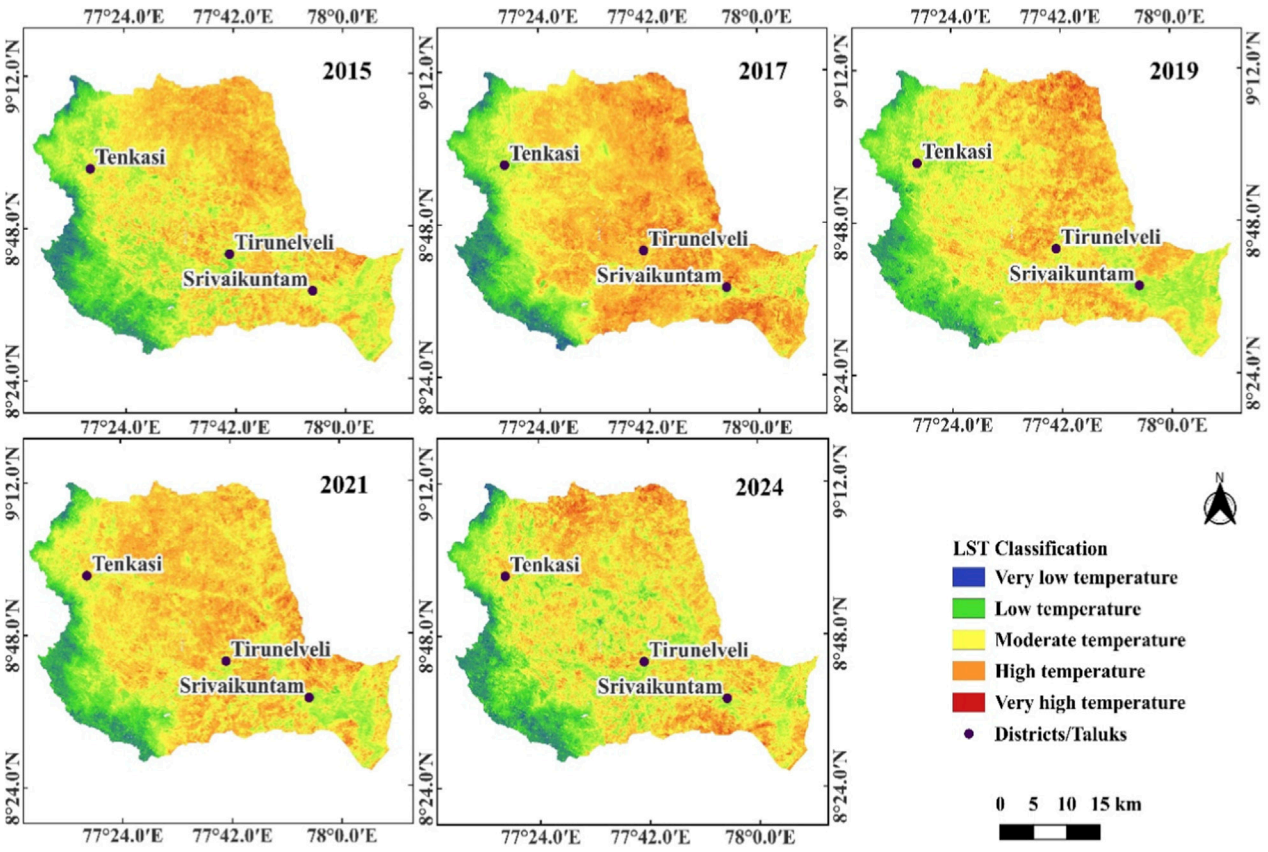


FIGURE 7
Annual average LST maps of Thamirabarani river basin in 5 years (2015, 2017, 2019, 2021, and 2024).

persistent cloud contamination, data for June, September, October, and November were excluded from the analysis in both years.

Figure 9a shows that, barren land, built-up land, and fallow land exhibited higher LST values during July and August, primarily due to reduced vegetation cover, extensive exposure of bare soils, and the prevalence of impervious surfaces. In contrast, the other LULC categories maintained moderate to low LSTs during most months, with cooler conditions prevailing outside the peak summer season. Densely vegetated areas consistently recorded lower LST values, reflecting the cooling effect of canopy cover, shading, and higher evapotranspiration rates.

In 2024 (Figure 9b), the highest LST values occurred in April, a pre-monsoon period characterized by dry climatic conditions, sparse vegetation, and limited soil moisture recharge, all of which contributed to intensified surface heating. The remaining months displayed low to moderate LST, associated with sparsely vegetated surfaces and seasonal climatic moderation. Overall, the comparison revealed an apparent intensification of LST across the barren, built-up, and fallow land classes, highlighting increasing thermal stress on non-vegetated surfaces. Conversely, vegetated areas continue to mitigate surface heating, underscoring their critical role in regulating land–atmosphere energy exchanges and buffering the impacts of climatic variability and land cover change.

3.5.3 Correlation between LULC and soil temperature

Figure 10 presents the correlation between ST and different LULC classes across multiple months for 2015 and 2024. In 2015 (Figure 10a), dense vegetation exhibited relatively low soil temperatures, primarily due to canopy shading, evapotranspiration, and enhanced soil moisture retention.

Agricultural areas recorded moderate ST values from March to September, coinciding with the dry season, when evapotranspiration rates were elevated and soil moisture availability declined. Barren land also showed moderate ST, reflecting the effect of sparse vegetation, where exposed surfaces absorbed heat during the day and released it rapidly at night, intensifying diurnal variability. Similarly, built-up areas displayed moderate ST during the same period, likely moderated by scattered vegetated patches and agricultural fields within settlement zones. During the monsoon season, the lowest ST values were observed across all classes, coinciding with peak rainfall from the northeast monsoon, which replenished soil moisture. Fallow lands and water bodies exhibited low to moderate ST values, while saltpans consistently showed higher ST values due to crystalline salt surfaces that trap heat and reflect solar radiation, thereby intensifying near-surface warming.

By 2024 (Figure 10b), a general increase in ST was observed across nearly all LULC classes. The rise was particularly evident in agricultural land, barren land, built-up land, fallow land, saltpans,

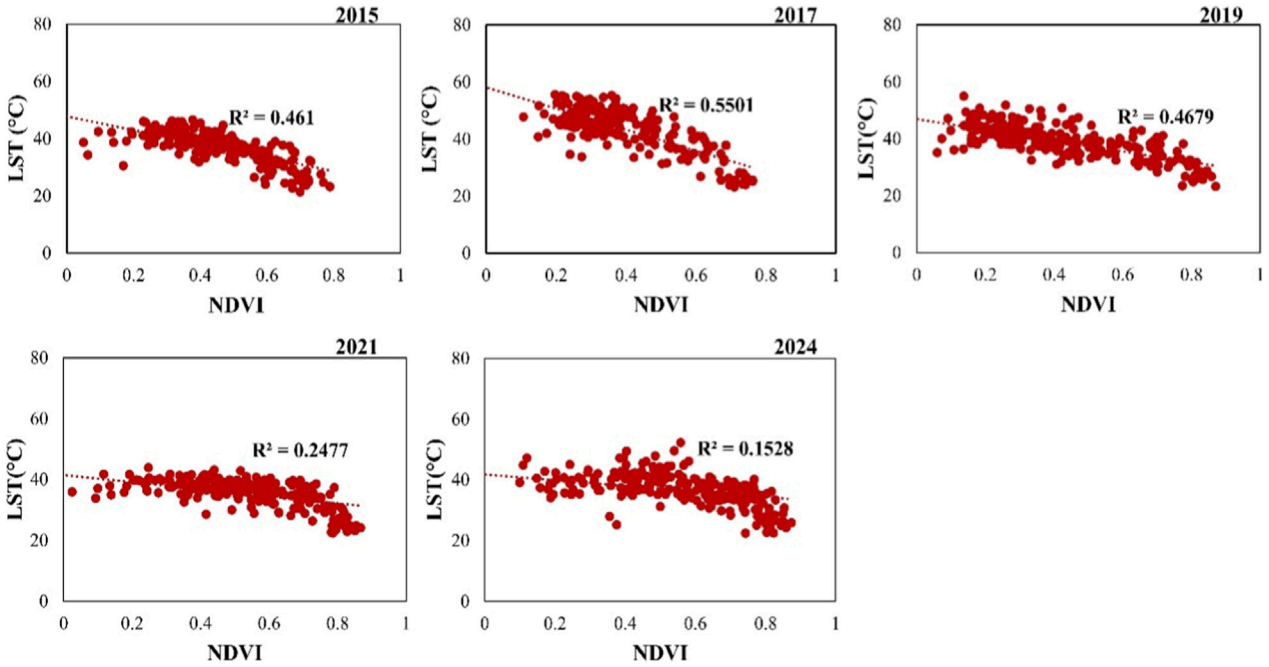


FIGURE 8
NDVI-LST correlation of Thamirabarani river basin in 5 years (2015, 2017, 2019, 2021, and 2024).

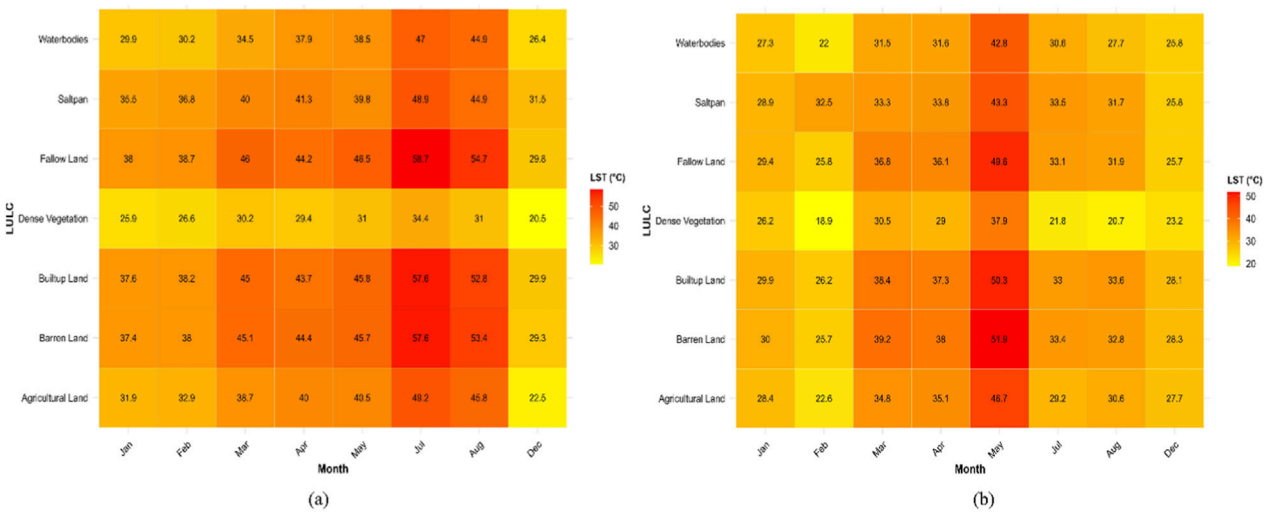


FIGURE 9
Relationship between LST and LULC classes in **(a)** 2015 and **(b)** 2024, represents the influence of each class with respect to land surface temperature.

and water bodies during April, a pre-monsoon month characterized by intense solar radiation, elevated air temperatures, and limited soil moisture recharge. In contrast, dense vegetation maintained lower soil temperatures, underscoring the buffering capacity of canopy cover and soil moisture storage in moderating land-atmosphere heat exchanges. The results from this study underscore the critical role of land cover type, seasonal variability, and climatic conditions in regulating soil thermal regimes. The observed warming trend across non-vegetated surfaces highlights increasing thermal stress over recent years, closely linked to climate variability, reduced soil moisture availability, and anthropogenic land-use changes.

4 Discussions

The Thamirabarani River Basin comprises diverse land cover types with agricultural land accounting for 57% of the total area (Kaliraj et al., 2024). The Thamirabarani River Basin has undergone

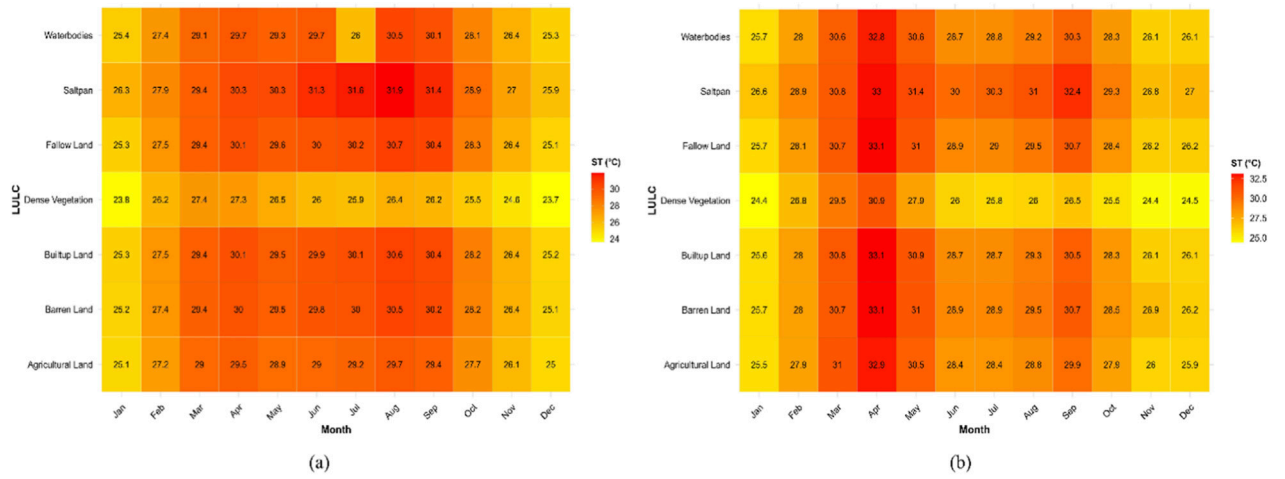


FIGURE 10
Relationship between ST and LULC classes in **(a)** 2015 and **(b)** 2024, represents the influence of each class with respect to soil temperature.

notable substantial transformations between 2015 and 2024, underscoring its vulnerability to agriculture stress, land degradation and climatic variability. The western part of the basin experiences high rainfall than the central and southeastern parts of the basin (Mohan Kumar et al., 2022). Therefore, western parts of the basin exhibited stable vegetation condition throughout the year. The concurrent rise in fallow land reflected increasing water scarcity, while marginal increases in built-up and barren land highlighted the effects of urban expansion and land degradation. Fluctuations in the extent of water bodies further underscored the consequences of deficit rainfall and urban sprawl, reinforcing the need for enhanced water management strategies (Ngondo et al., 2021). In addition, variability in saltpan areas in the downstream basin reflected human interventions that exacerbate local climatic pressures (Schauer et al., 2023). As shown in Figure 4, agricultural land maintained a stable condition and fallow land exhibited decreasing trends, whereas barren and built-up classes steadily increased, indicative of agricultural stress, settlement expansion and progressive land degradation. Variations in land use types and emissions of carbon serves as a primary factor contributing to temperature variations (Sun and Wu, 2025). The classification framework was robust, yielding overall accuracies above 80% and kappa coefficients ranging from strong to almost perfect agreement, thereby confirming the reliability of the classification results (Sellami and Rhinane, 2023).

The NDVI dynamics further demonstrated the influence of rainfall variability, agricultural stress, land degradation, and rising temperatures (Santhosh and Shilpa, 2023). Reduced soil moisture conditions negatively affected vegetation health, amplifying thermal and climatic stress across the basin. Although the long-term trend of NDVI indicated a slight but significant increase (slope = 0.00055, p = 0.0369) across the basin, this reflects vegetation fluctuations interrelated with seasonal and interannual dynamics. In contrast, spatial analysis revealed a stable vegetation condition across the basin over the period (2015-2024), with localized reduction in vegetation cover observed in built-up and degraded areas. The slight positive NDVI trend may indicate modest recovery in vegetation health, likely supported by cropping cycles and irrigation practices. The spatial distribution of LST was strongly modulated by land cover and topography. Higher LST values were consistently observed in settlement zones, reflecting the urban heat island effect. Meanwhile, the Western Ghats region maintained lower LST owing to dense vegetation cover and elevation-induced cooling. Rising temperatures in urban and agricultural areas intensified agricultural stress, highlighting the fragile nature of basin's ecosystems, where even minor climatic variations can have significant ecological consequences (Kaliraj et al., 2025; Kulkarni and Vijaya, 2021).

The correlation analysis of LST and NDVI revealed a negative correlation across years, consistent with urban heat-island effects (Jabbar and Yusoff, 2022). Weak correlations were associated with surface heterogeneity and rainfall variability, while moderate correlations reflected the close dependence of NDVI and LST on rainfall patterns and cropping cycles (Alademomi et al., 2020). Similar findings were reported in the Lower Son River Basin, where weak to moderate NDVI-LST correlations highlighted the coupled dynamics of vegetation health and surface temperature (Singh et al., 2024). Land-use changes, such as agricultural expansion, urbanization, and deforestation, significantly influence the relationship between NDVI and LST by altering vegetation cover and surface temperature regimes (Shamsudeen et al., 2022; Jiang et al., 2025). Moreover, areas with high NDVI have lower surface temperatures than areas with low NDVI, supporting spatial interpretation because vegetation acts as an efficient absorber of incoming radiation that is utilized for evapotranspiration and facilitates heat exchange between surface and atmosphere (Viju, 2023).

The correlation between LST-LULC classes revealed consistently higher values in barren, built-up, and fallow land classes, where limited vegetation precludes evaporative cooling. Conversely, vegetated areas and water bodies maintained lower LST, highlighting their role in local cooling (Ullah et al., 2023). The correlation between LULC and ST further emphasized vegetation's buffering capacity. Dense vegetation was associated with moderate ST, supported by evapotranspiration and soil

moisture storage. In contrast, barren land exhibited higher ST values due to limited soil moisture availability, while saltpans consistently recorded elevated ST because crystalline salt surfaces absorb and reflect solar energy (Safaee and Wang, 2020). Fallow lands and water bodies maintained lower ST values, reinforcing their role in local thermal moderation.

Overall, these findings indicate that LULC dynamics strongly regulate vegetation cover and surface thermal patterns. Expanding urban and barren areas intensify surface heating, increasing the risk of destabilizing the fragile basin ecosystem. The results emphasize the urgent need for integrated land and water management strategies, improved regulation of urban growth, and adaptive measures to enhance the basin's resilience to climate change. LULC, LST, ST, and LST-NDVI correlations were assessed for the entire basin, providing detailed insights into spatio-temporal shifts and identifying critical areas. Nevertheless, the study acknowledges certain limitations. Obtaining continuous, cloud-free datasets at specific temporal resolutions remains challenging, particularly during the monsoon season, when cloud cover is extensive, and data availability is limited. Additionally, processing long-term multi-sensor datasets is computationally intensive, which can constrain the scalability of such analyses in larger basins.

5 Conclusion

This study investigated LULC dynamics, vegetation variability, and the interactions of LST and ST with different LULC classes in the Thamirabarani River Basin. The LULC change detection results revealed that built-up land and barren land increased by 11.64% and 11.9%, respectively, highlighting rapid urban expansion and progressive land degradation within the basin. Analysis of NDVI maps also demonstrated fragmented losses in vegetation health, closely associated with the expansion of metropolitan areas and evidence of agricultural stress. Meanwhile, stable vegetation condition was observed in the western and southern parts of the basin, dominated by forest and farming areas. Long-term NDVI trend analysis indicated a slightly increasing but fluctuating pattern, reflecting the combined influence of seasonal variability and climatic drivers on vegetation dynamics. Similarly, LST maps effectively captured seasonal temperature variations, strongly influenced by land cover type and topographic conditions. Vegetated areas and water bodies consistently maintained lower LST and ST values due to shading, evapotranspiration, and moisture availability. In contrast, built-up and barren areas exhibited higher temperatures, reflecting the impacts of reduced vegetation, increased impervious surfaces, and land degradation.

Overall, the finding demonstrates that LULC transitions over the study period have severely affected vegetation patterns and that LULC plays a critical role in regulating both surface and soil temperatures. These results emphasize the far-reaching ecological consequences of land cover change, underscoring the need for sustainable land and water management practices to protect vegetation, mitigate land degradation, and preserve ecosystem balance.

Beyond scientific understanding, the outcomes of this study offer valuable applications for drought monitoring, precision agriculture, urban heat-island assessment, and climate change adaptation planning in the Thamirabarani River Basin. Future work should explore integrating high-resolution optical and hyperspectral datasets with advanced ML and deep learning techniques to enhance further the accuracy and reliability of LULC, NDVI, LST, and ST analyses.

Data availability statement

The original contributions presented in the study are included in the article/supplementary material, further inquiries can be directed to the corresponding authors.

Author contributions

PH: Investigation, Methodology, Software, Supervision, Writing – original draft. SG: Conceptualization, Data curation, Formal Analysis, Funding acquisition, Resources, Software, Visualization, Writing – original draft, Writing – review and editing. SJ: Investigation, Writing – original draft, Writing – review and editing. C-HH: Conceptualization, Data curation, Methodology, Writing – original draft.

Funding

The author(s) declared that financial support was received for this work and/or its publication. The work of C-HH was supported by the National Research Foundation of Korea (NRF) funded by the Korean Government (MSIT; RS-2025-00555756) and the Ministry of Education (RS-2018-NR031078).

Acknowledgements

The authors would like to acknowledge Karunya Institute of Technology and Sciences for providing the required facilities and logistical support during this research. We are very grateful to the reviewers for their comments and time on our paper.

Conflict of interest

Author SJ was employed by Geo Climate Risk Solutions Pvt. Ltd.

The remaining author(s) declared that this work was conducted in the absence of any commercial or financial relationships that could be construed as a potential conflict of interest.

Generative AI statement

The author(s) declared that generative AI was not used in the creation of this manuscript.

Any alternative text (alt text) provided alongside figures in this article has been generated by Frontiers with the support of artificial intelligence and reasonable efforts have been made to ensure accuracy, including review by the authors wherever possible. If you identify any issues, please contact us.

Publisher's note

All claims expressed in this article are solely those of the authors and do not necessarily represent those of their affiliated organizations, or those of the publisher, the editors and the reviewers. Any product that may be evaluated in this article, or claim that may be made by its manufacturer, is not guaranteed or endorsed by the publisher.

References

Abbas, Z., and Jaber, H. S. (2020). Accuracy assessment of supervised classification methods for extraction land use maps using remote sensing and GIS techniques. *IOP Conf. Ser. Mater. Sci. Eng.* 745 (1), 012166. doi:10.1088/1757-899X/745/1/012166

Abdalkadhum, A. J., Salih, M. M., and Jasim, O. Z. (2021). The correlation among land cover spectral indices and surface temperature using remote sensing techniques. *IOP Conf. Ser. Mater. Sci. Eng.* 1090 (1), 012024. doi:10.1088/1757-899x/1090/1/012024

Alademomi, A. S., Okolie, C. J., Daramola, O. E., Agboola, R. O., and Salami, T. J. (2020). Assessing the relationship of LST, NDVI and EVI with land cover changes in the Lagos lagoon environment. *Quaest. Geogr.* 39 (3), 87–109. doi:10.2478/quageo-2020-0025

Aldiansyah, S., and Saputra, R. A. (2023). Comparison of machine learning algorithms for land use and land cover analysis using google Earth engine (case study: Wanggu watershed). *Int. J. Remote Sens. Earth Sci. (IJReSES)* 19 (2), 197. doi:10.30536/j.ijreses.2022.v19.a3803

Amini, S., Saber, M., Rabiei-Dastjerdi, H., and Homayouni, S. (2022). Urban land use and land cover change analysis using random Forest classification of landsat time series. *Remote Sens.* 14 (11), 2654. doi:10.3390/rs14112654

Anitha, V., Devi, M. P., and Prabha, D. (2023). Bi-Temporal analysis of vegetation index on land surface temperature in Kottayam, Kerala. *Curr. World Environ.* 18 (3), 1065–1083. doi:10.12944/cwe.18.3.13

Asnawi, N. H., Kuok Choy, L., Che Rose, R. A., Widiawaty, M. A., Dede, M., and Muhammad, F. N. (2024). Impacts of urban land use and land cover changes on land surface temperature in Kuala Lumpur, Malaysia. *Malays. J. Soc. Space* 20 (1). doi:10.17576/geo-2024-2001-07

Bar, S., Parida, B. R., and Pandey, A. C. (2020). Landsat-8 and Sentinel-2 based Forest fire burn area mapping using machine learning algorithms on GEE cloud platform over Uttarakhand, Western Himalaya. *Remote Sens. Appl. Soc. Environ.* 18, 100324. doi:10.1016/j.rsase.2020.100324

Bento, V. A., Gouveia, C. M., DaCamara, C. C., Libonati, R., and Trigo, I. F. (2020). The roles of NDVI and Land Surface Temperature when using the Vegetation Health index over dry regions. *Glob. Planet. Change* 190, 103198. doi:10.1016/j.gloplacha.2020.103198

Binh, N. A., Nhut, H. S., An, N. N., Phuong, T. A., Hanh, N. C., Thao, G. T. P., et al. (2021). Thirty-year dynamics of LULC at the dong thap muoi area, southern Vietnam, using google earth engine. *ISPRS Int. J. Geo-Information* 10 (4), 226. doi:10.3390/ijgi10040226

Digra, M., Dhir, R., and Sharma, N. (2022). Land use land cover classification of remote sensing images based on the deep learning approaches: a statistical analysis and review. *Arabian J. Geosciences* 15 (10), 1003. doi:10.1007/s12517-022-10246-8

El Garouani, M., Amyay, M., Lahrach, A., and Jarar Oulidi, H. (2021). Exploring the relationship between LST, LULC and NDVI in saïss plain using geospatial techniques. *E3S Web Conf.* 314, 04001. doi:10.1051/e3sconf/202131404001

Ermida, S. L., Soares, P., Mantas, V., Göttsche, F. M., and Trigo, I. F. (2020). Google earth engine open-source code for land surface temperature estimation from the landsat series. *Remote Sens.* 12 (9), 1471. doi:10.3390/RS12091471

Feizizadeh, B., Omarzadeh, D., Kazemi Garajeh, M., Lakes, T., and Blaschke, T. (2023). Machine learning data-driven approaches for land use/cover mapping and trend analysis using Google Earth Engine. *J. Environ. Plan. Manag.* 66 (3), 665–697. doi:10.1080/09640568.2021.2001317

Feng, S., Li, W., Xu, J., Liang, T., Ma, X., Wang, W., et al. (2022). Land Use/Land cover mapping based on GEE for the monitoring of changes in ecosystem types in the upper yellow River Basin over the Tibetan Plateau. *Remote Sens.* 14 (21), 5361. doi:10.3390/rs14215361

Gaur, S., and Singh, R. (2023). A comprehensive review on land Use/Land cover (LULC) change modeling for urban development: current status and future prospects. *Sustain. Switz.* 15 (Issue 2), 903. doi:10.3390/su15020903

Gelata, F. T., Jiqin, H., Gemeda, S. C., and Asefa, B. W. (2023). Application of GIS using NDVI and LST estimation to measure climate variability-induced drought risk assessment in Ethiopia. *J. Water Clim. Change* 14 (7), 2479–2489. doi:10.2166/wcc.2023.154

Guechi, I., Gherraz, H., and Alkama, D. (2021). Relationship between lulc characteristic and lst using remote sensing and gis, case study guelma (algeria). *Rev. Roum. Géogr./Rom. Journ. Geogr.* 65 (Issue 2). Available online at: https://www.researchgate.net/publication/357780794.

Guha, S., and Govil, H. (2021). An assessment on the relationship between land surface temperature and normalized difference vegetation index. *Environ. Dev. Sustain.* 23 (2), 1944–1963. doi:10.1007/s10668-020-00657-6

Guha, S., and Govil, H. (2022). Seasonal variability of LST-NDVI correlation on different land use/land cover using Landsat satellite sensor: a case study of Raipur City, India. *Environ. Dev. Sustain.* 24 (6), 8823–8839. doi:10.1007/s10668-021-01811-4

Guha, S., Govil, H., and Diwan, P. (2020a). Monitoring LST-NDVI relationship using premonsoon landsat datasets. *Adv. Meteorology* 2020, 1–15. doi:10.1155/2020/4539684

Guha, S., Govil, H., Gill, N., and Dey, A. (2020b). Analytical study on the relationship between land surface temperature and land use/land cover indices. *Ann. GIS* 26 (2), 201–216. doi:10.1080/19475683.2020.1754291

Gunawan, R. A. R., Hadibasyir, H. Z., and Arijuddin, B. I. (2023). Analysis of the impact of residential land development on LST in Semarang City, 421–435. doi:10.2991/978-2-38476-066-4_27

Gündüz, H. İ. (2025). Land-Use land-cover dynamics and future projections using GEE, ML, and QGIS-MOLUSCE: a case Study in Manisa. *Sustain. Switz.* 17 (4), 1363. doi:10.3390/su17041363

Ho, C.-H., Park, S.-J., Jeong, S.-J., Kim, J., and Jhun, J.-G. (2012). Observational evidences of double cropping impacts on the climate in the northern China plains. *J. Clim.* 25, 4721–4728. doi:10.1175/jcli-d-11-00224.1

Hu, Y., Raza, A., Syed, N. R., Acharki, S., Ray, R. L., Hussain, S., et al. (2023). Land Use/Land cover change detection and NDVI estimation in Pakistan's Southern Punjab Province. *Sustain. Switz.* 15 (4), 3572. doi:10.3390/su15043572

Imroah, F. F. K., and Setiawan, N. (2024). Integration of Landsat-8 OLI/TIRS and Sentinel-1A PolSAR for analyzing land surface temperature and its anomalies linked to ENSO in Surakarta, Indonesia. *Geomatica* 76 (2), 100038. doi:10.1016/j.geomat.2024.100038

IPCC (2023). "Climate change 2023: synthesis report. Contribution of working groups I, II and III to the sixth assessment report of the intergovernmental Panel on climate change," in *Core writing team*. Editors Lee, H., and Romeo, J. (Geneva, Switzerland: IPCC), 184. doi:10.59327/IPCC/AR6-9789291691647

Jabbar, M., and Yusoff, M. M. (2022). Assessing the spatiotemporal urban green cover changes and their impact on land surface temperature and urban heat island in Lahore (Pakistan). *Geogr. Environ. Sustain.* 15 (1), 130–140. doi:10.24057/2071-9388-2021-005

Jackson, P. G., Goel, P., and Singh, S. (2025). "Prediction of land use and land cover using Google Earth Engine (GEE) and machine learning algorithms: a review," in *2025 IEEE international conference on interdisciplinary approaches in technology and management for social innovation, IATMSI 2025*. doi:10.1109/IATMSI64286.2025.10984782

Jamei, Y., Seyedmahmoudian, M., Jamei, E., Horan, B., Mekhilef, S., and Stojcevski, A. (2022). Investigating the relationship between land Use/Land cover change and land surface temperature using Google Earth engine; case Study: melbourne, Australia. *Sustain. Switz.* 14 (22), 14868. doi:10.3390/su142214868

Jangid, A., Gupta, M. K., and Shrivastava, V. (2023). Techniques and challenges of the machine learning method for land Use/Land cover (LU/LC) classification in remote sensing using the Google Earth engine. *Int. J. Recent Innovation Trends Comput. Commun.* 11 (7), 85–92. doi:10.17762/ijritcc.v11i7.7833

Jeong, S.-J., Ho, C.-H., and Jeong, J.-H. (2009). Increased vegetation activity and decreased springtime regional warming over East Asia. *Geophys. Res. Lett.* 36, L02710. doi:10.1029/2008GL036583

Jeong, S.-J., Ho, C.-H., Piao, S., Kim, J., Ciais, P., Lee, Y.-B., et al. (2014). Effects of double cropping on summer climate of the North China Plain and neighboring regions. *Nat. Clim. Change* 4, 615–619. doi:10.1038/nclimate2266

Jiang, R., Dong, Y., Bai, L., Dong, W., and Qu, A. (2025). Predicting urban residents' climate change risk perceptions: the role of heat and green space exposure indicators in Harbin's residential environment. *Sustain. Cities Soc.* 134, 106882. doi:10.1016/j.scs.2025.106882

Kaliraj, S., Srinivas, R., Kiruthika, N., Vairaveni, E., Mohamed, H., Palanivel, K., et al. (2024). "Remote sensing indices based soil properties measurement–a case study of the Thamirabarani River Basin, South India," in *Remote sensing of soils* (Elsevier), 45–63.

Kaliraj, S., Krishnan, K. A., Suresh, D., Kasivisvanathan, K. S., and Chandrasekar, N. (2025). Evaluating soil erosion patterns and potential impacts of rainfall and vegetation index in the semi-arid river basin of southern India. *Environ. Monit. Assess.* 197, 848. doi:10.1007/s10661-025-14277-y

Khachoo, Y. H., Cutugno, M., Robustelli, U., and Pugliano, G. (2024). Impact of land use and land cover (LULC) changes on carbon stocks and economic implications in Calabria using Google Earth Engine (GEE). *Sensors* 24 (17), 5836. doi:10.3390/s24175836

Khan, A., Alamgir, A., and Fatima, N. (2025). Spatiotemporal analysis of land use and land cover changes, LST and NDVI in Thatta district, Sindh, Pakistan. *Kuwait J. Sci.* 52 (1), 100326. doi:10.1016/j.kjs.2024.100326

Kulkarni, K., and Vijaya, P. A. (2021). "Correlating land surface temperature with LULC, vegetation index and topography," in *2021 international conference on circuits, controls and communications, CCUBE 2021*. doi:10.1109/CCUBE53681.2021.9702712

Liu, C., Li, W., Zhu, G., Zhou, H., Yan, H., and Xue, P. (2020). Land use/land cover changes and their driving factors in the northeastern tibetan plateau based on geographical detectors and google earth engine: a case study in gannan prefecture. *Remote Sens.* 12 (19), 3139. doi:10.3390/RS12193139

Liu, Y., Qiu, H., Wang, N., Yang, D., Zhao, K., Yang, G., et al. (2025). Thermokarst disturbance responses to climate change across the circumpolar permafrost regions from 1990 to 2023. *Geosci. Front.* 16, 102147. doi:10.1016/j.gsf.2025.102147

Loukika, K. N., Keesara, V. R., and Sridhar, V. (2021). Analysis of land use and land cover using machine learning algorithms on google earth engine for Munneru river basin, India. *Sustain. Switz.* 13 (24), 13758. doi:10.3390/su132413758

Mansourmoghaddam, M., Rousta, I., Cabral, P., Ali, A. A., Olafsson, H., Zhang, H., et al. (2023). Investigation and prediction of the land Use/Land cover (LU/LC) and Land Surface Temperature (LST) changes for Mashhad City in Iran during 1990–2030. *Atmosphere* 14 (4), 741. doi:10.3390/atmos14040741

Mohan Kumar, S., Geethalakshmi, V., Ramanathan, S., Senthil, A., Senthilraja, K., Bhuvaneswari, K., et al. (2022). Rainfall spatial-temporal variability and trends in the Thamirabharani River Basin, India: implications for agricultural planning and water management. *Sustain. Switz.* 14 (22), 14948. doi:10.3390/su142214948

Nasiri, V., Deljouei, A., Moradi, F., Sadeghi, S. M. M., and Borz, S. A. (2022). Land use and land cover mapping using Sentinel-2, Landsat-8 satellite images, and Google Earth engine: a comparison of two composition methods. *Remote Sens.* 14 (9), 1977. doi:10.3390/rs14091977

National Water Commission (2017). Thamirabarani River Basin report. Available online at: https://nwm.gov.in/.

Ngondo, J., Mango, J., Liu, R., Nobert, J., Dubi, A., and Cheng, H. (2021). Land-use and land-cover (Lulc) change detection and the implications for coastal water resource management in the wami–ruvu basin, Tanzania. *Sustain. Switz.* 13 (8), 4092. doi:10.3390/su13084092

Nigar, A., Li, Y., Jat Baloch, M. Y., Alrefaei, A. F., and Almutairi, M. H. (2024). Comparison of machine and deep learning algorithms using Google Earth Engine and Python for land classifications. *Front. Environ. Sci.* 12, 1378443. doi:10.3389/fenvs.2024.1378443

Nikkala, S., Peddada, J. R., and Neredimelli, R. (2022). Correlation analysis of land surface temperature on landsat-8 data of Visakhapatnam Urban Area, Andhra Pradesh, India. *Earth Sci. Inf.* 15 (3), 1963–1975. doi:10.1007/s12145-022-00850-3

Njoku, E. A., and Tenenbaum, D. E. (2022). Quantitative assessment of the relationship between land use/land cover (LULC), topographic elevation and land surface temperature (LST) in Ilorin, Nigeria. *Remote Sens. Appl. Soc. Environ.* 27, 100780. doi:10.1016/j.rsase.2022.100780

Nse, O. U., Okolie, C. J., and Nse, V. O. (2020). Dynamics of land cover, land surface temperature and NDVI in Uyo City, Nigeria. *Sci. Afr.* 10, e00599. doi:10.1016/j.sciaf.2020.e00599

Pan, X., Wang, Z., Gao, Y., Dang, X., and Han, Y. (2022). Detailed and automated classification of land use/land cover using machine learning algorithms in Google Earth Engine. *Geocarto Int.* 37 (18), 5415–5432. doi:10.1080/10106049.2021.1917005

Pande, C. B. (2022). Land use/land cover and change detection mapping in Rahuri watershed area (MS), India using the google earth engine and machine learning approach. *Geocarto Int.* 37 (26), 13860–13880. doi:10.1080/10106049.2022.2086622

Pande, C. B., Diwate, P., Orimoloye, I. R., Sidek, L. M., Pratap Mishra, A., Moharir, K. N., et al. (2024). Impact of land use/land cover changes on evapotranspiration and model accuracy using Google Earth engine and classification and regression tree modeling. *Geomatics, Nat. Hazards Risk* 15 (1), 2290350. doi:10.1080/19475705.2023.2290350

Park, C.-E., Jeong, S.-J., Ho, C.-H., Park, H., Piao, S., Kim, J., et al. (2017). Dominance of climate warming effects on recent drying trends over wet monsoon regions. *Atmos. Chem. Phys.* 17, 10467–10476. doi:10.5194/acp-17-10467-2017

Park, H., Jeong, S.-J., Ho, C.-H., Park, C.-E., and Kim, J. (2018). Slowdown of spring green-up advancements in boreal forests. *Remote Sens. Environ.* 217, 191–202. doi:10.1016/j.rse.2018.08.012

Patel, D. K., Thakur, T. K., Thakur, A., Pandey, A., Kumar, A., Kumar, R., et al. (2024a). Quantifying land degradation in upper catchment of Narmada River in central India: evaluation study utilizing landsat imagery. *Water* 16 (17), 2440. doi:10.3390/w16172440

Patel, D. K., Thakur, T. K., Thakur, A., Karuppannan, S., Swamy, S. L., and Pant, R. R. (2024b). Groundwater potential zone mapping using AHP and geospatial techniques in the upper Narmada basin, central India. *Discov. Sustain.* 5 (1), 355. doi:10.1007/s43621-024-00560-4

Patel, S., Indraganti, M., and Jawarneh, R. N. (2024c). A comprehensive systematic review: impact of Land Use/Land Cover (LULC) on Land Surface Temperatures (LST) and outdoor thermal comfort. *Build. Environ.* 249, 111130. doi:10.1016/j.buildenv.2023.111130

Patil, A., and Panhalkar, S. (2023). A comparative analysis of machine learning algorithms for land use and land cover classification using google earth engine platform. *J. Geomatics* 17 (2), 226–233. doi:10.58825/jog.2023.17.2.96

Pokhariya, H. S., Singh, D. P., and Prakash, R. (2023). Evaluation of different machine learning algorithms for LULC classification in heterogeneous landscape by using remote sensing and GIS techniques. *Eng. Res. Express* 5 (4), 045052. doi:10.1088/2631-8695/acfa64

Qu, L., Chen, Z., Li, M., Zhi, J., and Wang, H. (2021). Accuracy improvements to pixel-based and object-based LULC classification with auxiliary datasets from google earth engine. *Remote Sens.* 13 (3), 453. doi:10.3390/rs13030453

Rahimi, E., Dong, P., and Jung, C. (2025). Global NDVI-LST Correlation: Temporal and Spatial Patterns from 2000 to 2024. *Environ. - MDPI* 12 (2), 67. doi:10.3390/environments12020067

Rehman, A., Qin, J., Pervez, A., Khan, M. S., Ullah, S., Ahmad, K., et al. (2022). Land-Use/Land cover changes contribute to land surface temperature: a case Study of the upper indus Basin of Pakistan. *Sustain. Switz.* 14 (2), 934. doi:10.3390/su14020934

Safaee, S., and Wang, J. (2020). Towards global mapping of salt pans and salt playas using Landsat imagery: a case study of Western United States. *Int. J. Remote Sens.* 41 (22), 8693–8716. doi:10.1080/01431161.2020.1781285

Sajan, B., Kanga, S., Singh, S. K., Mishra, V. N., and Durin, B. (2023). Spatial variations of LST and NDVI in muzaffarpur district, Bihar using google earth engine (GEE) during 1990-2020. *J. Agrometeorology* 25 (2), 262–267. doi:10.54386/jam.v25i2.2155

Santhosh, L. G., and Shilpa, D. N. (2023). Assessment of LULC change dynamics and its relationship with LST and spectral indices in a rural area of bengaluru district, Karnataka India. *Remote Sens. Appl. Soc. Environ.* 29, 100886. doi:10.1016/j.rsase.2022.100886

Schauer, H., Schlaffer, S., Bueechi, E., and Dorigo, W. (2023). Inundation–desiccation state prediction for salt pans in the Western pannonian basin using remote sensing, groundwater, and meteorological data. *Remote Sens.* 15 (19), 4659. doi:10.3390/rs15194659

Sellami, E. M., and Rhinane, H. (2023). A new approach for mapping land use/land cover using google Earth engine: a comparison of composition images. *Int. Archives Photogrammetry, Remote Sens. Spatial Inf. Sci. - ISPRS Archives* 48 (4/W6-2022), 343–349. doi:10.5194/isprs-archives-XLVIII-4-W6-2022-343-2023

Shafizadeh-Moghadam, H., Khazaei, M., Alavipanah, S. K., and Weng, Q. (2021). Google Earth engine for large-scale land use and land cover mapping: an object-based classification approach using spectral, textural and topographical factors. *GIScience Remote Sens.* 58 (6), 914–928. doi:10.1080/15481603.2021.1947623

Shamsudeen, M., Padmanaban, R., Cabral, P., and Morgado, P. (2022). Spatio-temporal analysis of the impact of landscape changes on vegetation and land surface temperature over Tamil Nadu. *Earth* 3 (2), 614–638. doi:10.3390/earth3020036

Shanmugam, V., Kandasamy, S., and Radhakrishnan, R. (2022). Identification of drought risk areas in preceding season of *rabi* crops in the vellar river basin, Tamil Nadu, India. *Arab. J. Geosci.* 15, 1210. doi:10.1007/s12517-022-10465-z

Sharma, M., Bangotra, P., Gautam, A. S., and Gautam, S. (2022). Sensitivity of normalized difference vegetation index (NDVI) to land surface temperature, soil moisture and precipitation over district gautam buddh Nagar, UP, India. *Stoch. Environ. Res. Risk Assess.* 36 (6), 1779–1789. doi:10.1007/s00477-021-02066-1

Sharmin, T., Chappell, A., and Lannon, S. (2024). Spatio-temporal analysis of LST, NDVI and SUHI in a coastal temperate city using local climate zone. *Energy Built Environ.* 6, 1142–1155. doi:10.1016/j.enbenv.2024.06.002

Singh, S., Kumar, P., Parijat, R., Gonengcil, B., and Rai, A. (2024). Establishing the relationship between land use land cover, normalized difference vegetation index and land surface temperature: a case of Lower son river basin, India. *Geogr. Sustain.* 5 (2), 265–275. doi:10.1016/j.geosus.2023.11.006

Sohail, M. T., Manzoor, Z., Ehsan, M., Al-Ansari, N., Khan, M. B., Shafi, A., et al. (2023). Impacts of urbanization, LULC, LST, and NDVI changes on the static water table with possible solutions and water policy discussions: a case from Islamabad, Pakistan. *Front. Environ. Sci.* 11, 1018500. doi:10.3389/fenvs.2023.1018500

Sun, R., and Wu, X. (2025). Extremes of diurnal temperature range in karst regions: definition, trends and interaction with wind speed. *Atmos. Res.* 327, 108379. doi:10.1016/j.atmosres.2025.108379

Talukdar, S., Singha, P., Mahato, S., Shahfahad, P. , S., Liou, Y. A., Rahman, A., et al. (2020). Land-use land-cover classification by machine learning classifiers for satellite observations-A review, *Remote Sens.* 12. 1135. doi:10.3390/rs12071135

Tassi, A., Gigante, D., Modica, G., di Martino, L., and Vizzari, M. (2021). Pixel- vs. Object-based landsat 8 data classification in google earth engine using random forest: the case study of Maiella national park. *Remote Sens.* 13 (12), 2299. doi:10.3390/rs13122299

Tewabe, D., and Fentahun, T. (2020). Assessing land use and land cover change detection using remote sensing in the Lake Tana Basin, Northwest Ethiopia. *Cogent Environ. Sci.* 6 (1), 1778998. doi:10.1080/23311843.2020.1778998

Thakur, T. K., Patel, D. K., Saini, S., Thakur, A., Swamy, S. L., Bakshi, S., et al. (2025a). A geospatial analysis of coal mine overburden reclamation: land use, carbon stock, biomass, and soil genesis in chronosequence plantations. *J. Geochem. Explor.* 271, 107674. doi:10.1016/j.gexplo.2025.107674

Thakur, T. K., Patel, D. K., Thakur, A., and Arora, N. K. (2025b). Evaluation of land degradation vulnerability in coal mined areas of Madhya Pradesh, India using geospatial and AHP modeling: a 40-year assessment and eco-restoration of degraded landscape. *Environ. Sustain.* 8 (1), 85–101. doi:10.1007/s42398-025-00347-x

Thi Hong Ngoc, T., Duc Thang, N., and Truong Khanh, P. (2025). Analysis of the urban heat Island phenomenon in Chau Doc City, An Giang Province, Vietnam. *Int. J. Environ. Sci.* 11 (18), 1806–1821. doi:10.64252/zc21cb90

Ullah, W., Ahmad, K., Ullah, S., Tahir, A. A., Javed, M. F., Nazir, A., et al. (2023). Analysis of the relationship among land surface temperature (LST), land use land cover (LULC), and normalized difference vegetation index (NDVI) with topographic elements in the lower Himalayan region. *Heliyon* 9 (2), e13322. doi:10.1016/j.heliyon.2023.e13322

Viju, T., C, M. F., and V, S. K. (2023). Assessment of land surface temperature variations and implications of land Use/Land cover changes: a case of Malappuram Urban agglomeration Region, Kerala, India. *Int. J. Built Environ. Sustain.* 10 (3), 13–36. doi:10.11113/ijbes.v10.n3.1102

Wang, M., He, G., Hu, T., Yang, M., Zhang, Z., Zhang, Z., et al. (2024). Innovative hybrid algorithm for simultaneous land surface temperature and emissivity retrieval: case study with SDGSAT-1 data. *Remote Sens. Environ.* 315, 114449. doi:10.1016/j.rse.2024.114449

Yaghoobi, M., Vafaeenejad, A., Moradi, H., and Hashemi, H. (2022). Analysis of landscape composition and configuration based on LULC change modeling. *Sustain. Switz.* 14 (20), 13070. doi:10.3390/su142013070

Yue, W., Xu, J., Tan, W., and Xu, L. (2007). The relationship between land surface temperature and NDVI with remote sensing: application to Shanghai Landsat 7 ETM+ data. *Int. Journal Remote Sensing* 28 (15), 3205–3226. doi:10.1080/01431160500306906

Zhang, M., Zhang, C., Kafy, A. A., and Tan, S. (2021). Simulating the relationship between land use/cover change and urban thermal environment using machine learning algorithms in wuhan city, China. *Land* 11 (1), 14. doi:10.3390/land11010014